ISOLATED BIDIRECTIONAL MICROINVERTER WITH PROPORTIONAL RESONANT CONTROLLER FOR RENEWABLE ENERGY SYSTEM

Mr. N.Pandikumar, PG scholar, M.E Power Electronics,
Mr. M.Sivaraman, M.E., Assistant Professor,
P.S.R Engineering College, Sevalpatti, Sivakasi-626 140.

ABSTRACT:

A single-stage single-phase isolated bidirectional microinverter based on proportional resonant (PR) controlled is proposed in this project. With the PR-PWM control, the voltage conversion ratio of the resonant converter can be regulated from zero to infinite, theoretically, which means the PR-PWM is suitable for wide voltage range applications, such as single-stage isolated inverters. Moreover, the voltage conversion ratio of the resonant converter is only determined by the equivalent duty cycle and free of the value and direction of the transferred power. Therefore, the value and direction of the power flow can be changed smoothly, which makes the proposed converter suitable for bidirectional DC/AC power conversion. Accordingly, a simple unified current controller can be employed for both inverter mode and rectifier mode. In addition, soft switching can be achieved during most of the grid period and high efficiency can be achieved with the proposed solution. Detailed operation principles, characteristics, design considerations and control strategy of the proposed microinverter are presented.

I - INTRODUCTION

Due to the accelerating energy shortage and the exhaustion of global resources, renewable energy, such as photovoltaic (PV) and electrical vehicles (EVs), have been receiving a persistent interest, especially in the residential area. However, the conflict between production and consumption of solar energy is a fundamental problem for homeowners: energy consumption is highest in the morning and evening while solar production peaks during midday. The surplus solar energy is consumed by batteries to mitigate the influence of excess solar energy. When needed, the energy stored in the batteries will be released to supply the load. If necessary, the EV car can also help to power the load. The bidirectional grid-connected DC/AC converter is the key to achieve energy management.

For grid-connected applications, galvanic isolation is a basic requirement for safety considerations. Isolated DC/AC converters can be categorized into two groups, i.e. two-stage and single-stage converters. Compared with two-stage solutions, a single-stage solution can directly convert DC to line-frequency AC with only one-stage conversion, resulting in reduced power switches, higher efficiency and minimized high DC voltage indoors. Since the parasitic resistance of battery at low frequency is very small, the double-line-frequency ripple is induced in the charging current with the single stage solutions. Many researches have been conducted on the impact of double-line-frequency current ripple. These researches indicate that the double-line-frequency current ripple has little influence in terms of capacity, cell balancing, and temperature rise and roundtrip efficiency. In this case, it is unnecessary to suppress the double-line-frequency current ripple, which will greatly reduce the DC-link capacitors. Hence, a more competitive cost, higher efficiency and higher power density can be achieved with single-stage DC/AC converters, which have drawn an increasing attention in recent years.

Although an increasing effort has been made on the study of single-stage DC/AC solutions over the years, the single stage DC/AC converters still face many challenges: 1) wide operating voltage range not only on battery side but also on grid side, 2) isolated bidirectional conversion, 3) changing the direction of transferred power quickly. Particularly, the grid voltage changes from zero to hundreds of volts. A buck-type or boost-type converter is not suitable for bidirectional DC/AC power conversion due to limited voltage conversion range.
Hence, the bidirectional single-stage DC/AC converter is still an emergent research topic.

A bidirectional single-stage inverter is based on the bidirectional fly back converter. However, disadvantages of the fly back converter, i.e. hard switching, high voltage and current stresses, make it not a good candidate for high efficiency power conversion. By integrating a high frequency transformer, a series of buck-type bidirectional inverter are derived from conventional non-isolated H-bridge inverters. However, these topologies suffer from large voltage spikes and low efficiency induced by the leakage inductance of transformer. A voltage clamped circuit is employed to recycle the

energy stored in leakage inductance. But too much auxiliary components result in reduced power density.

II - LITERATURE REVIEW

L. Zhang, et. al., (2018) presents, a grid-tied photovoltaic (PV) generation system based on series-connected module integrated inverters (SC-MIIs. In the grid-tied SC-MII system, each PV panel is interfaced with a MII with independent maximum power point tracking (MPPT) to harvest maximum solar energy. The outputs of MIIs are at AC line frequency and are connected in series to fulfill the voltage requirement in the utility grid. Since the high step-up power conversion stage in the conventional micro-inverter is avoided, the grid-tied SC-MII system is easier to implement and features high efficiency.

A. Pal et. al., (2019) presents a novel single-stage soft switched high frequency link three-phase DC-AC converter topology. The topology supports unidirectional DC to AC power flow and is targeted for applications like grid integration of photovoltaic sources, fuel cell etc. The high frequency magnetic isolation results in reduction of system volume, weight and cost. Sine-wave pulse width modulation is implemented in DC side converter. Though high frequency switched, DC side converter is soft-switched for most part of the line cycle. The AC side converter active switches are line frequency switched incurring negligible switching loss.

III - SYSTEM IMPLEMENTATION

1. PROPOSED SYSTEM

In this project proposed a bidirectional resonant converter with PR controller system for renewable energy applications. Based on the basic principle of PR-PWM controlled resonant converter, a solution for a single-stage isolated bidirectional microinverter is proposed.

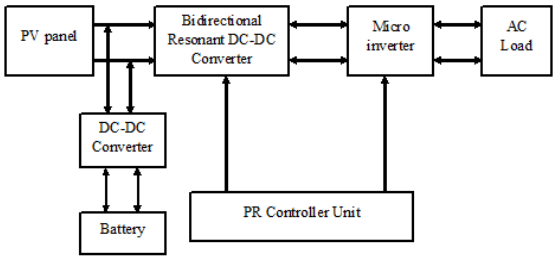

Fig.1 Proposed system Block

The major advantage of the proposed solution are as follows: 1) The voltage gain can be theoretically regulated from zero to infinite, which helps to avoid the zero-crossing issue of the isolated single-stage DC/AC converter based on the LLC converters. 2) The voltage gain is only determined by the duty cycle and free of the transferred power. 3) The amplitude and direction of transferred power can be changed quickly. A unified current controller can be employed, which is much simpler than the single-stage DC/AC solutions based on the bidirectional resonant converters.

2. PROPOSED BIDIRECTIONAL MICROINVERTER

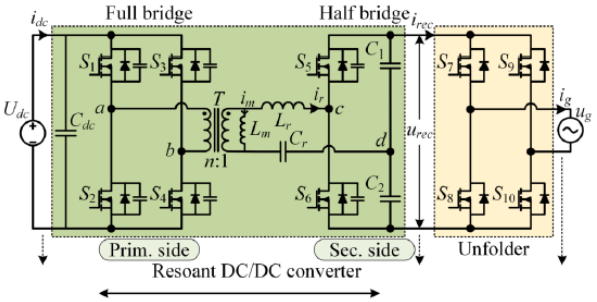

Fig.2 The proposed bidirectional microinverter

Fig.2 illustrates the proposed single-stage isolated bidirectional converter. It is composed of two parts, i.e., a resonant DC/DC converter and a line-frequency unfolding inverter (unfolder). The resonant converter consists of a full bridge in the primary side and a half bridge in the secondary side, linked by a high-frequency transformer T, a resonant inductor Lr and a resonant capacitor Cr. Since the DC voltage is relatively low and higher voltage conversion ratio is required for the bidirectional DC/AC converter, a half bridge is employed in the secondary side of the converter to reduce the turn's ratio of the high frequency transformer. The main purpose of the resonant converter is to regulate the output current and achieve power factor correction (PFC). While the unfolder is employed to reconstruct the pseudo-DC-link current to sinusoidal AC current. Both the resonant converter and the unfolder support bidirectional power flow.

For LLC converters, the voltage conversion ratio is independent of the load only when it operates at resonant frequency. Inspired by this characteristic, the propose converter always operates at the resonant frequency, which is expressed as (1).

$$f_r = \frac{1}{2\pi\sqrt{L_r C_r}} \quad (1)$$

The state function of the resonant current i_r and the voltage u_{Cr} across the resonant capacitor can be expressed as (2).

$$\begin{cases} L_r \frac{di_r}{dt} = u_{ab} - u_{cd} - u_{Cr} \\ C_r \frac{du_{Cr}}{dt} = i_r \end{cases} \quad (2)$$

where uab and ucd are the midpoint voltages of primary side and secondary side, respectively. Considering the fundamental

component of i_r and u_{Cr}, the state function (2) can be simplified and written as (3).

$$U_{ab1} - U_{cd1} = j\omega_s L_r L_{r1} + \frac{I_{r1}}{j\omega_s C_r} \quad (3)$$

where !s is the angular frequency at switching frequency.

U_{ab1} and U_{cd1} are the fundamental component of u_{ab} and u_{cd}, respectively.

When the converter operates at the resonant frequency, the fundamental impedance of the resonant tank equals to zero. In this case, $U_{ab1} = U_{cd1}$, which means that U_{ab1} and U_{cd1} have not only the same amplitude but also the same phase. Accordingly, the midpoint voltages u_{ab} and u_{cd} of primary side and secondary side also share the same phase.

3. Operation Principles of control strategy

The normalized voltage conversion ratio is expressed as (4). According to the voltage conversion ratio, the proposed converter is divided into two modes, i.e. buck mode and boost mode. The converter operates in the buck mode when $M_n \leq 1$ while operates in the boost mode when $M_n > 1$.

$$M_n = \frac{nu_{rec}}{2U_{dc}} \quad (4)$$

where n is the turns ratio of the transformer.

The operation mode of the proposed converter can also be divided into forward mode and backward mode according to the direction of power flow. In the forward mode, the energy stored in the batteries is transferred to the grid. The proposed converter operates as an inverter. In the backward mode, the converter draws energy from the grid and transmit it to the DC side. The proposed converter operates as a rectifier.

1) Boost Mode:

In the boost mode, the duty cycle of the primary-side switches is fixed to 0.5. The output current is regulated by the duty cycle of the secondary-side switches. Fig.3 illustrates the typical waveforms of the boost mode. The switches in the same leg are driven complementary. The gating signals of S1, S4 and S5 are in phase. The gating signals of S2, S3 and S6 are in phase as well.

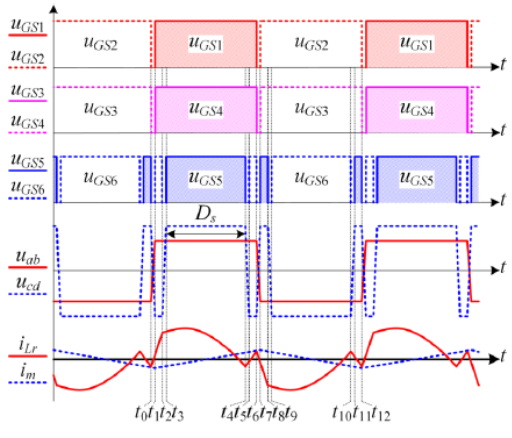

(a)

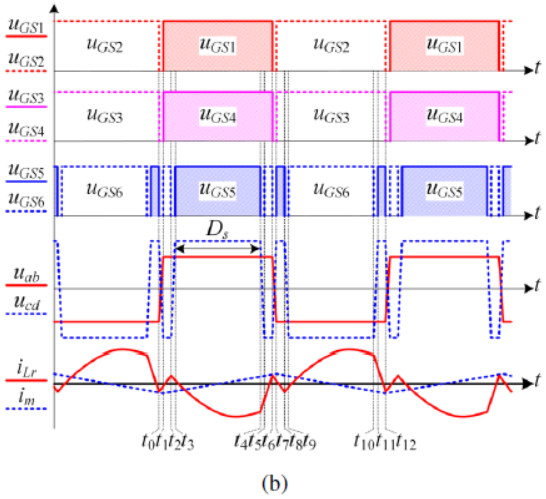

(b)

Fig.3 Typical operating waveforms of the resonant DC/DC converter in boost mode: (a) forward mode, (b) backward mode.

In order to ensure symmetrical drive of S5 and S6, the switching sequence is S6-S5-S6 in the positive half switching period and t2 - t1 = t6 - t5. The drive in the negative half switching period is symmetrical to that in the positive half switching period. Since the operation principles of the forward mode and the backward mode are similar, only the forward mode is discussed in detail.

Fig.3 (a) illustrates the typical waveforms in the forward mode and boost mode. Each switching period can be divided into twelve stages. The equivalent circuits of these stages are shown in Fig.4.

Stage I [t0-t1] [Fig.4(a)]: Before t0, S2, S3 and S5 are ON. The midpoint voltage u_{ab} of primary-side bridge is clamped to $-U_{dc}$ while the voltage u_{cd} is clamped to u_{rec}=2. The resonant current i_r and magnetizing current i_m are negative. At t0, the switches S2, S3 and S5 are turned off. Due to the negative current, the parasitic capacitors of S2, S3 and S5 are charged while that of S1, S4 and S6 are discharged. Until u_{ab} reaches U_{dc}, the parasitic diodes of S1, S4 and S6 are forced to be conducted and ZVS can be achieved.

Stage II [t1 - t2] [Fig..4(b)]: At t1, the switches S1, S2 and S6 are turned on with ZVS. u_{ab} is clamped to U_{dc} while u_{cd} is clamped to $-u_{rec}/2$. The resonant current i_r increase quickly due to a large positive voltage $U_{dc}=n+u_{rec}/2$ applied on resonant tank. The magnetizing current i_m also increases linearly.

During Stage I and Stage II, u_{cd} is clamped to $-u_{rec}/2$. Therefore, the input voltage charges the resonant tank quickly. The resonant current i_r and the voltage u_{Cr} across the resonant capacitor Cr can be calculated by (5) and (6).

$$i_r(t) = i_r(t_0)\cos\omega_r(t-t_0) + \frac{\frac{U_{dc}}{n}+\frac{U_{rec}}{2}-u_{Cr}(t_0)}{Z_r}\sin\omega_r(t-t_0) \quad (5)$$

$$u_{Cr}(t) = i_r(t_0)Z_r \sin\omega_r(t-t_0) + \frac{U_{dc}}{n} + \frac{U_{rec}}{2} - \left(\frac{U_{dc}}{n} + \frac{U_{rec}}{2} - u_{Cr}(t_0)\right)\cos\omega_r(t-t_0) \quad (6)$$

where $\omega_r = 2\pi fr$ is the angular frequency and $Z_r = \sqrt{L_r/C_r}$ is the characteristic impedance of the series-resonant tank.

Stage III [t2 - t3] [Fig.4(c)]: At t2, S6 is turned off. The parasitic capacitor of S6 is charged by the positive resonant current and the parasitic capacitor of S5 is discharged. Since the resonant current is relatively large, S5 can easily achieve ZVS.

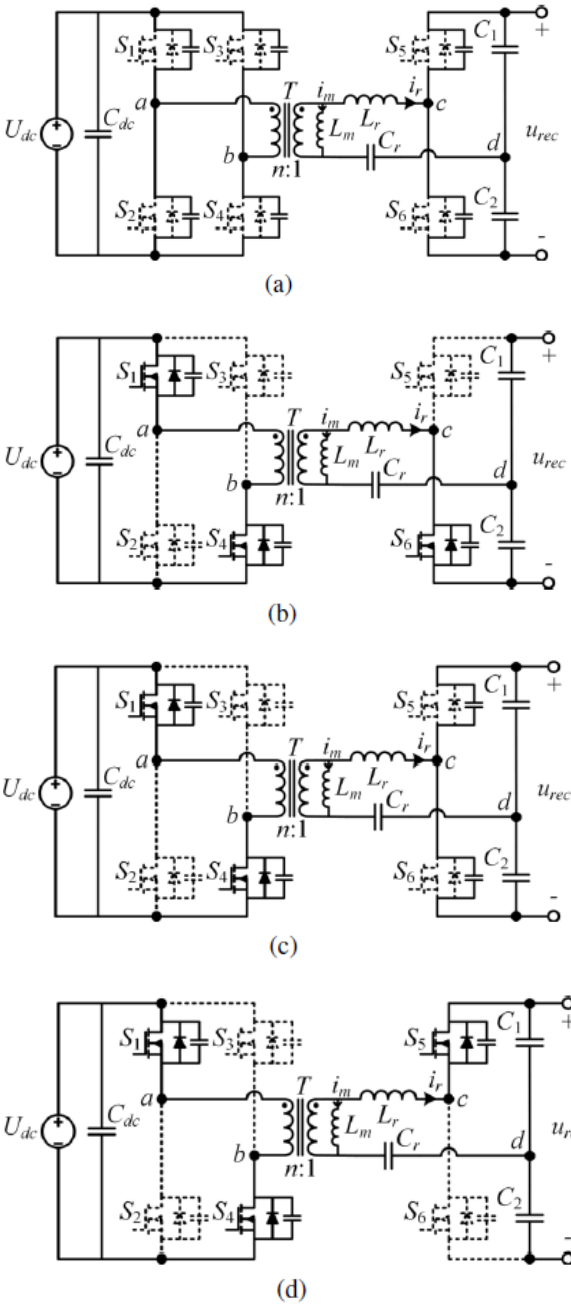

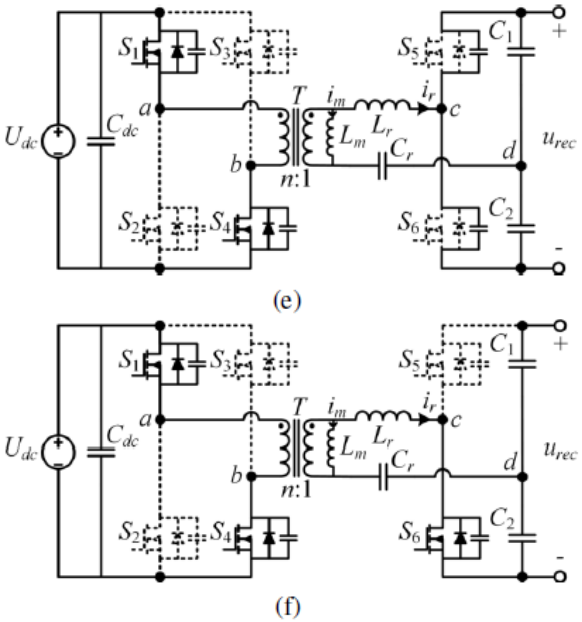

Fig.4 Equivalent circuits of the resonant DC/DC converter in boost mode: (a) [t0 - t1], (b) [t1 - t2], (c) [t2 - t3], (d) [t3 - t4], (e) [t4 - t5], (f) [t5 - t6].

Stage IV [t3 - t4] [Fig.4(d)]: At t3, S5 is turned on with ZVS. u_{cd} is clamped to $u_{rec}/2$. The resonant inductor L_r resonants with the resonant capacitor Cr together. i_m keeps increasing linearly due to the positive voltage u_{ab} clamped to U_{dc}. During the two stages, L_r resonates with C_r. Most of the power is transferred during these two stages. i_r and u_{Cr} can be expressed as (7) and (8).

$$i_r(t) = i_r(t_2)\cos\omega_r(t-t_2) + \frac{\frac{U_{dc}}{n} - \frac{U_{rec}}{2} - u_{Cr}(t_2)}{Z_r}\sin\omega_r(t-t_2) \quad (7)$$

$$u_{Cr}(t) = i_r(t_2)Z_r \sin\omega_r(t-t_2) + \frac{U_{dc}}{n} - \frac{U_{rec}}{2} - \left(\frac{U_{dc}}{n} - \frac{U_{rec}}{2} - u_{Cr}(t_2)\right)\cos\omega_r(t-t_2) \quad (8)$$

Stage V [t4 - t5] [Fig. 3.4(e)]: At t4, S5 is turned off. The negative resonant current charges the parasitic capacitor of S5 and discharges the parasitic capacitor of S6. Until u_{cd} is reduced to $-u_{rec}/2$, the body diode of S6 is conducted and ZVS can be achieved at light load. However, the resonant current is reduced and close to zero at heavy load. It is difficult for S6 to achieve ZVS at t5. But fortunately, ZCS of S6 can still be achieved.

Stage VI [t5 - t6] [Fig. 3.4(f)]: At t5, S6 is turned on with ZCS. The resonant current increases due to a positive voltage applied on the series-resonant tank. During Stage V and Stage VI, u_{cd} is clamped to $-u_{rec}/2$. i_r and u_{Cr} can be calculated by (9) and (10).

$$i_r(t) = i_r(t_4)\cos\omega_r(t-t_4) + \frac{\frac{U_{dc}}{n} + \frac{U_{rec}}{2} - u_{Cr}(t_4)}{Z_r}\sin\omega_r(t-t_4) \quad (9)$$

$$u_{Cr}(t) = i_r(t_4)Z_r \sin\omega_r(t-t_4) + \frac{U_{dc}}{n} + \frac{U_{rec}}{2} - \left(\frac{U_{dc}}{n} + \frac{U_{rec}}{2} - u_{Cr}(t_4)\right)\cos\omega_r(t-t_4) \quad (10)$$

The operation principles of the rest stages are symmetrical to the positive half switching period and will not be discussed again.

2) Buck Mode:

In the buck mode, the switches in secondary side always operate with a duty cycle of 0.5 while the duty cycle of the switches in primary side is modulated to regulate the output. Fig.5 shows typical waveforms of the buck mode. The operation principle of the buck mode is similar to that of the boost mode.

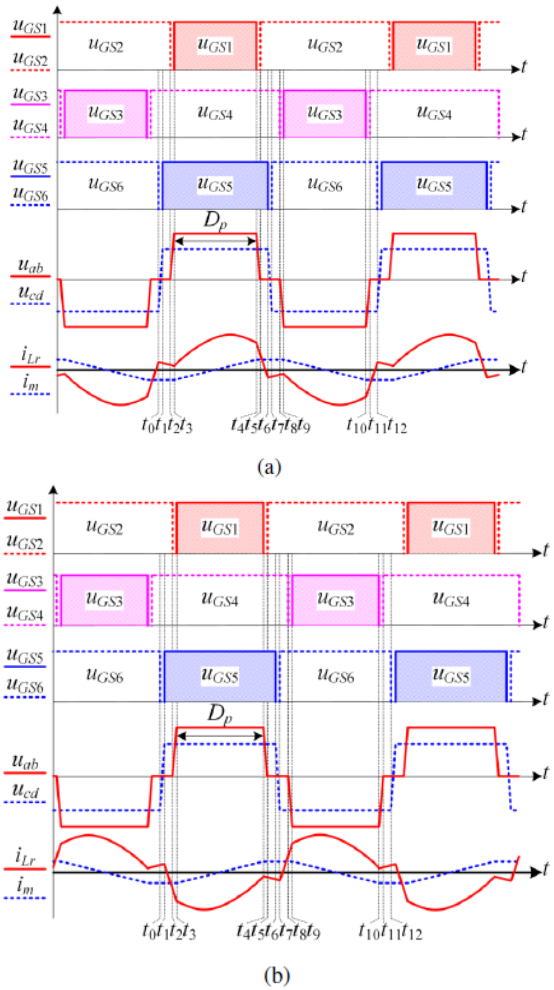

Fig.5 Typical operating waveforms of the resonant DC/DC converter in buck mode: (a) forward mode, (b) backward mode.

4. PROPORTIONAL-RESONANT (PR) CONTROLLER

The proportional-resonant (PR) controller is one of the most popular controllers used for grid-connected inverters to regulate the current injected into the grid. In this chapter, the PR current controller is designed and implemented for three-phase inverters, in the stationary reference frame and in the natural reference frame.

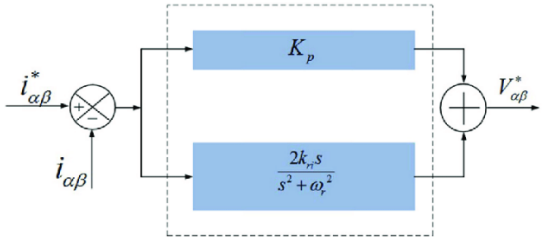

Fig.6 Proportional-resonant Controller

For inverters, the controller deals with sinusoidal signals, which makes it difficult to design the controller with the correct gain that is able to regulate the performance at the fundamental frequency and also to reject harmonic disturbances. PI controllers, having a pole (with an infinite gain) at the zero frequency, are not able to eliminate the steady-state error at the fundamental frequency unless it is adopted in the *dq* frame. A PR controller is the combination of a proportional term and a resonant term given by

$$C_{PR}(s) = K_p + K_i \frac{s}{s^2+\omega^2}$$

where ω is the resonant frequency. Such a controller has a high gain around the resonant frequency and, thus, is capable of eliminating the steady-state error when tracking or rejecting a sinusoidal signal, according to the internal model principle.

5. HARDWARE PRESENTATION

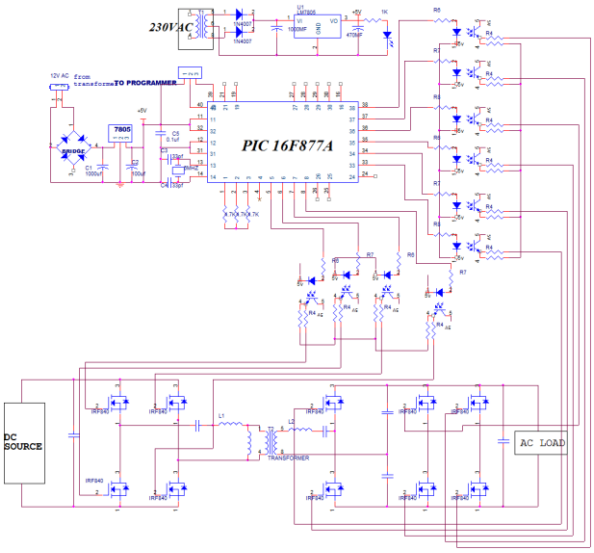

Fig.7 Circuit diagram

In this figure.7 we are design a micro inverter with embedded controller system. The proposed single-stage isolated bidirectional converter consists of two parts, i.e., a resonant DC/DC converter and a line-frequency unfolding inverter (unfolder). The output

of this circuit is connected to the loads. The converter and inverter designed with MOSFETS. The each MOSFET are connected with the opto coupler which is connected with the controller ports. The controller we are using are is PIC 16F877A.

A. PIC16F877A BOARD:

PIC –Peripheral Interface Controller

PIC 16F877 is one of the most advanced microcontroller from Microchip. This controller is widely used for experimental and modern applications because of its low price, wide range of applications, high quality, and ease of availability. It is ideal for applications such as machine control applications, measurement devices, study purpose, and so on.

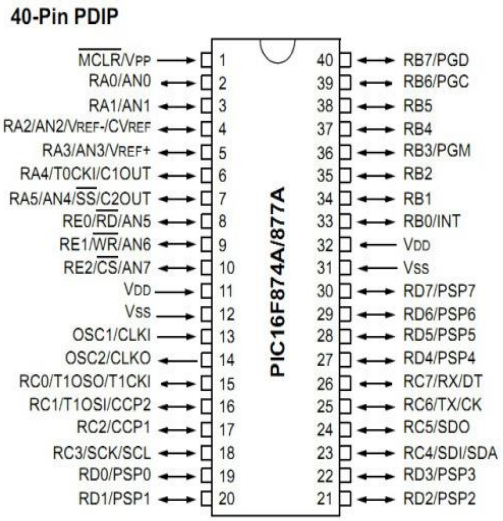

Figure.8 PIC16F877a

B. OPTO COUPLER

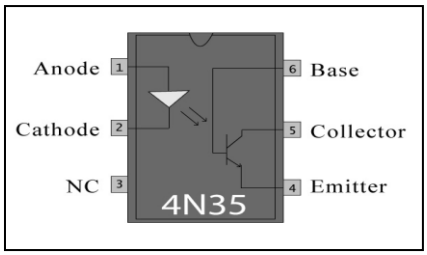

Figure.9 Pin Diagram – 4N35

In electronics, an **opto-isolator**, also called an **optocoupler**, **photocoupler**, or **optical isolator**, is "an electronic device designed to transfer electrical signals by utilizing light waves to provide coupling with electrical isolation between its input and output". The main purpose of an opto-isolator is "to prevent high voltages or rapidly changing voltages on one side of the circuit from damaging components or distorting transmissions on the other side."

C. MOSFET

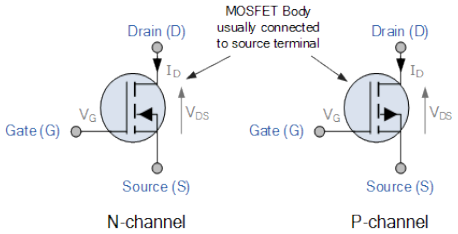

Figure.10 Symbol – IRF840

Third generation Power MOSFETs from Vishay provide the designer with the best combination of fast switching, ruggedized device design, low on-resistance and cost-effectiveness.

- Dynamic dV/dt Rating
- Repetitive Avalanche Rated
- Fast Switching
- Ease of Paralleling
- Simple Drive Requirements
- Compliant to RoHS Directive 2002/95/EC

IV - RESULTS & DISCUSSION

The proposed system model that is designed in MATLAB 2014a Simulink platform. The following figure.11 represents proposed Simulink model.

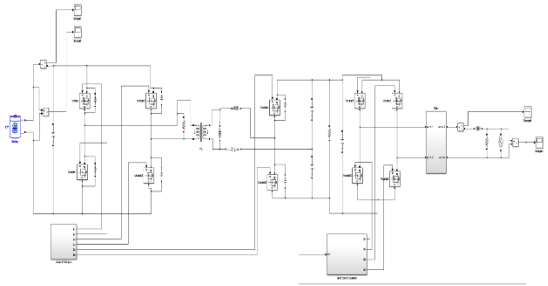

Fig.11 Proposed system model

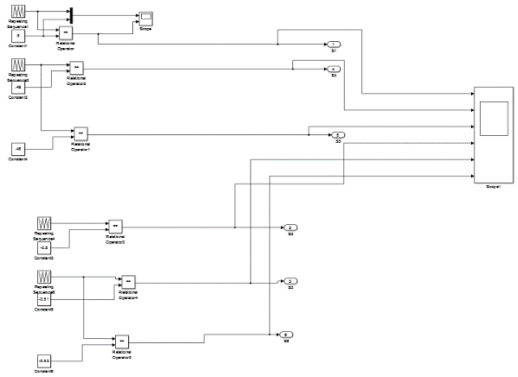

Fig.12 PWM Control

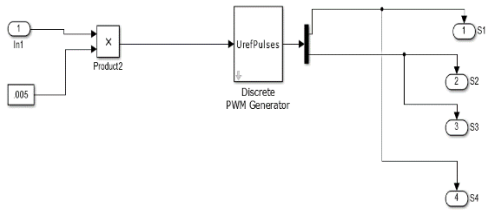

Fig.13 Control system

The following figure.14 represents the battery DC voltage. Battery gives the DC voltage at 40V.

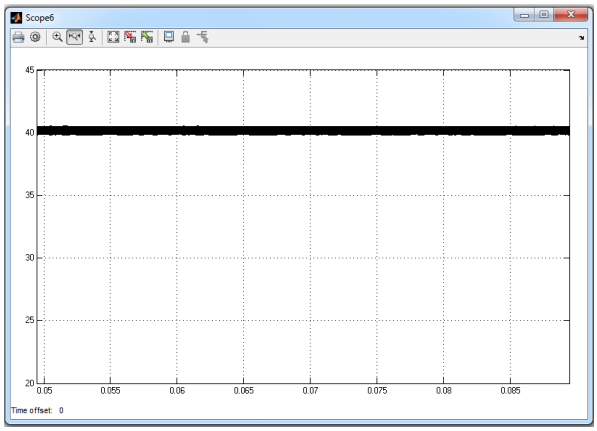

Fig.14 Battery voltage

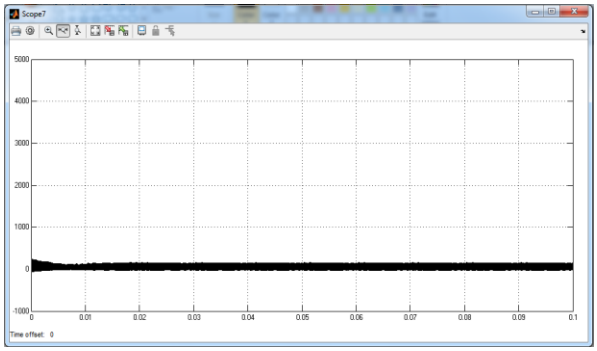

Fig.15 Battery current

The following figure.16 shown the PWM gate signal. Ramp and sine wave generate the PWM pulse signal.

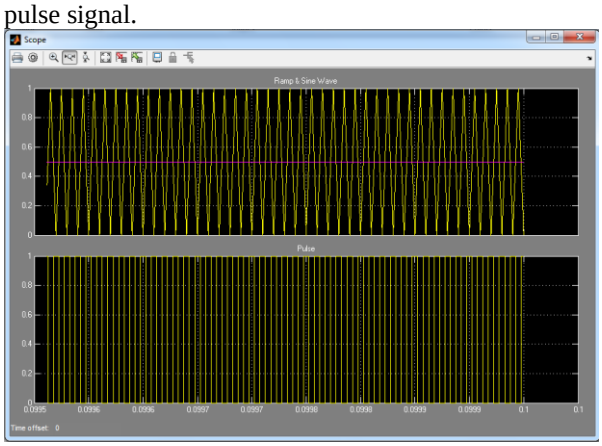

Fig.16 Ramp & Sine wave

The following figure.17 represents the grid output AC voltage. Battery voltage is given to resonant converter and inverter. Inverter gives AC voltage and is injected to grid. It produces 230V AC.

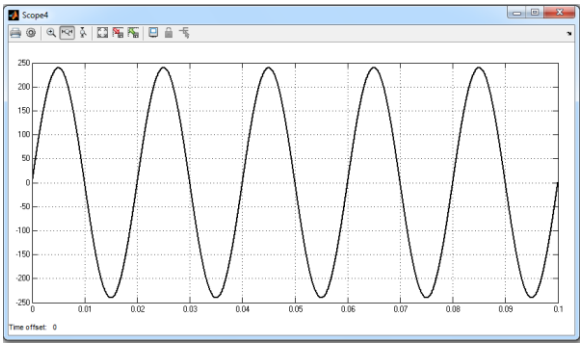

Fig.17 Output AC voltage

The following figure.18 shown the grid output current. It reached at 6A.

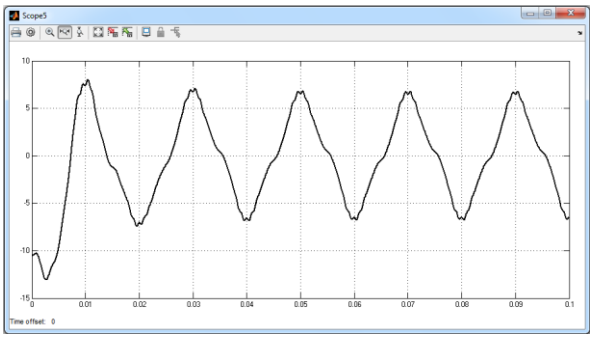

Fig.18 Output current

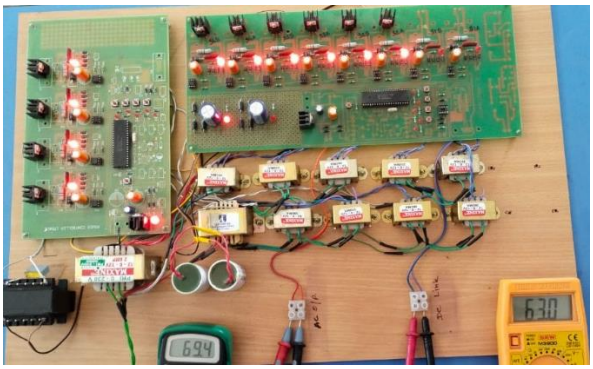

Fig.19 Hardware kit

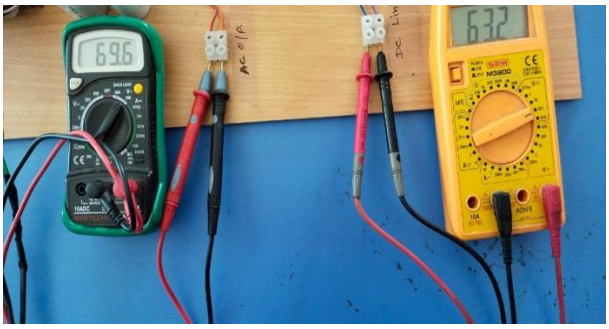

Fig.20 DC link output 63.2 and AC output voltage 69.6

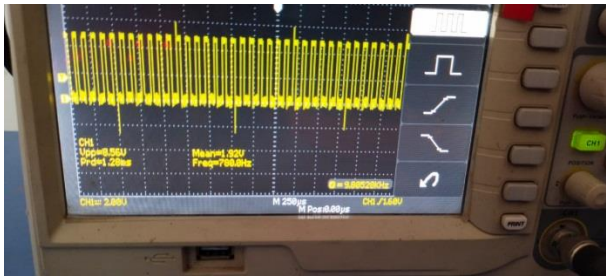

Fig.21 High frequency inverter gate pulse

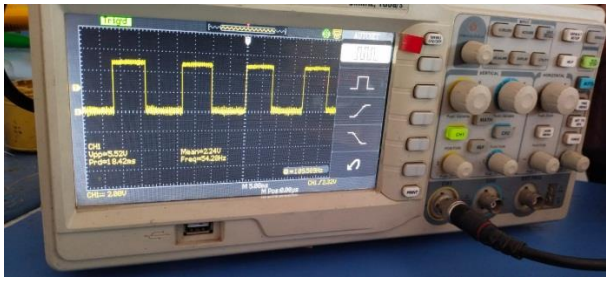

Fig.22 Inverter 50Hz Switch pulse

V - CONCLUSION

In this project, a single-stage single-phase isolated bidirectional microinverter based on the PR based controlled resonant converter is proposed and investigated for energy storage applications. With the PR-PWM control, the voltage conversion ratio of the resonant converter is able to vary a wide range and both step-up and -down voltage conversion are achieved. The amplitude and direction of the transferred power can be changed quickly and smoothly with a simple unified current controller. Soft-switching has also been achieved during most of the grid period. The modelling of PR (proportional resonant) controller for an isolated bidirectional microinverter and observation of its performance during load fluctuation condition is done using MATLAB/Simulink and verify the results in hardware presentation.

REFERENCES

[1] B. K. Bose, "Global energy scenario and impact of power electronics in 21st century," IEEE Trans. Power Electron., vol. 60, no. 7, pp. 2638-2651, Jul. 2013.

[2] L. Zhang, K. Sun, Y. W. Li, X. Lu, and J. Zhao, "A Distributed Power Control of Series-connected Module Integrated Inverters for PV Gridtied Applications," IEEE Trans. Power Electron., vol. 33, no. 9, pp. 7698-7707, Sep. 2018.

[3] H. B. Hu, S. Harb, N. Kutkut, I. Batarseh, and Z. J. Shen, "A Review of Power Decoupling Techniques for Microinverters With Three Different Decoupling Capacitor Locations in PV Systems," IEEE Trans. Power Electron., vol. 28, no. 6, pp. 2711-2726, Jun 2013.

[4] A. Pal and K. Basu, "A Unidirectional Single-Stage Three-Phase Soft-Switched Isolated DC–AC Converter," IEEE Trans. Power Electron., vol. 34, no. 2, pp. 1142-1158, 2019.

[5] S. Bala, T. Tengn´er, P. Rosenfeld and F. Delince, "The effect of low frequency current ripple on the performance of a Lithium Iron Phosphate (LFP) battery energy storage system," in Proc. IEEE Energy Convers. Congr. Expo., Raleigh, NC, 2012, pp. 3485-3492.

[6] T. H. Kim, J. B. Jeong, B. H. Lee, D. H. Shin, H. S. Song, B. H. Ki, H. J. Kim, "Analytical study on low-frequency ripple effect of battery charging," in Proc. IEEE Veh. Power Propuls. Conf., Seoul, 2012, pp. 809-811.

[7] H. Z. Z. Beh, G. A. Covic and J. T. Boys, "Effects of pulse and DC charging on lithium iron phosphate (LiFePO4) batteries," in Proc. IEEE Energy Convers. Congr. Expo., Denver, CO, 2013, pp. 315-320.

[8] Y. S. Jeong, S. H. Lee, S. G. Jeong, J. M. Kwon, and B. H. Kwon, "High-Efficiency Bidirectional Grid-Tied Converter Using Single Power Conversion With High-Quality Grid Current," IEEE Trans. Ind. Electron., vol. 64, no. 11, pp. 8504-8513, Nov 2017.

[9] P. T. Krein, R. S. Balog, and X. Geng, "High-frequency link inverter for fuel cells based on multiple-carrier PWM," IEEE Trans. Power Electron., vol. 19, no. 5, pp. 1279-1288, Sep 2004.

[10] J. R. Kan, S. J. Xie, Y. Y. Wu, Y. Tang, Z. L. Yao, and R. Chen, "High-Frequency-Link Inverter Using Combined Synchronous Rectifiers," IEEE Trans. Ind. Electron., vol. 61, no. 12, pp. 6769-6777, Dec 2014.

[11] R. K. Surapaneni, D. B. Yelaverthi, and A. K. Rathore, "Cycloconverter- Based Double-Ended Microinverter Topologies for Solar Photovoltaic AC Module," IEEE J. Emerg. Sel. Topics Power Electron., vol. 4, no. 4, pp. 1354-1361, Dec 2016.

[12] W. J. Zhu, K. L. Zhou, and M. Cheng, "A Bidirectional High-Frequency-Link Single-phase Inverter: Modulation, Modeling, and Control," IEEE Trans. Power Electron., vol. 29, no. 8, pp. 4049-4057, Aug 2014.

[13] S. Zhong, J. P. Xu, and X. Zhou, "High-Efficiency Zero-Voltage Switching Single-Stage Switching Amplifier With Half-Bridge Active Clamping Circuit," IEEE Trans. Ind. Electron., vol. 65, no. 11, pp. 8574-8584, Nov 2018.

[14] N. D. Weise, G. Castelino, K. Basu, and N. Mohan, "A Single-Stage Dual-Active-Bridge-Based Soft Switched AC-DC Converter With Open- Loop Power Factor Correction and Other Advanced Features," IEEE Trans. Power Electron., vol. 29, no. 8, pp. 4007-4016, Aug 2014.

